Pure Appl. Chem., Vol. 83, No. 1, pp. 95–110, 2011.
doi:10.1351/PAC-CON-10-10-25

Graphene oxide as surfactant sheets*

Laura J. Cote, Jaemyung Kim, Vincent C. Tung, Jiayan Luo, Franklin Kim, and Jiaxing Huang‡

Department of Materials Science and Engineering, Northwestern University, Evanston, IL 60208, USA

Abstract: Graphite oxide sheet, now referred to as graphene oxide (GO), is the product of chemical oxidation and exfoliation of graphite powders that was first synthesized over a century ago. Interest in this old material has resurged in recent years, especially after the discovery of graphene, as GO is considered a promising precursor for the bulk production of graphene-based materials. GO sheets are single atomic layers that can readily extend up to tens of microns in lateral dimension. Therefore, their structure bridges the typical length scales of both chemistry and materials science. GO can be viewed as an unconventional type of soft material as it carries the characteristics of polymers, colloids, membranes, and as highlighted in this review, amphiphiles. GO has long been considered hydrophilic due to its excellent water dispersity, however, our recent work revealed that GO sheets are actually amphiphilic with an edge-to-center distribution of hydrophilic and hydrophobic domains. Thus, GO can adhere to interfaces and lower interfacial energy, acting as surfactant. This new property insight helps to better understand GO's solution properties which can inspire novel material assembly and processing methods such as for fabricating thin films with controllable microstructures and separating GO sheets of different sizes. In addition, GO can be used as a surfactant sheet to emulsify organic solvents with water and disperse insoluble materials such as graphite and carbon nanotubes (CNTs) in water, which opens up opportunities for creating functional hybrid materials of graphene and other π-conjugated systems.

Keywords: amphiphiles; graphene oxide; interfaces; Langmuir–Blodgett technique; monolayers; surfactants.

INTRODUCTION

According to the IUPAC Gold Book, graphene is a single carbon layer of the graphite structure analogous to a polycyclic aromatic hydrocarbon of quasi-infinite size [1]. It is a two-dimensional crystal consisting of a single atomic layer of sp^2-hybridized carbon atoms (Fig. 1a). In 2004, it was isolated by mechanical exfoliation from graphite crystal and visualized under an optical microscope by Andre Geim and Konstantin Novoselov [2]. This has triggered the explosive growth of interest in this new material across many disciplines, which has led to the discovery of many extraordinary properties [3]. For example, graphene was found to have high optical transparency of 97.7 %, high electron mobility of up to 200 000 $cm^2 \cdot V^{-1} \cdot s^{-1}$, high thermal conductivity of up to 5000 $W \cdot m^{-1} \cdot K^{-1}$, high nominal surface area of 2630 m^2/g, and high breaking strength of 42 N/m. Therefore, many exciting applications

Pure Appl. Chem.* **83, 1–252 (2011). A collection of invited, peer-reviewed articles by former winners of the IUPAC Prize for Young Chemists, in celebration of the International Year of Chemistry 2011.

‡Corresponding author: E-mail: Jiaxing-huang@northwestern.edu

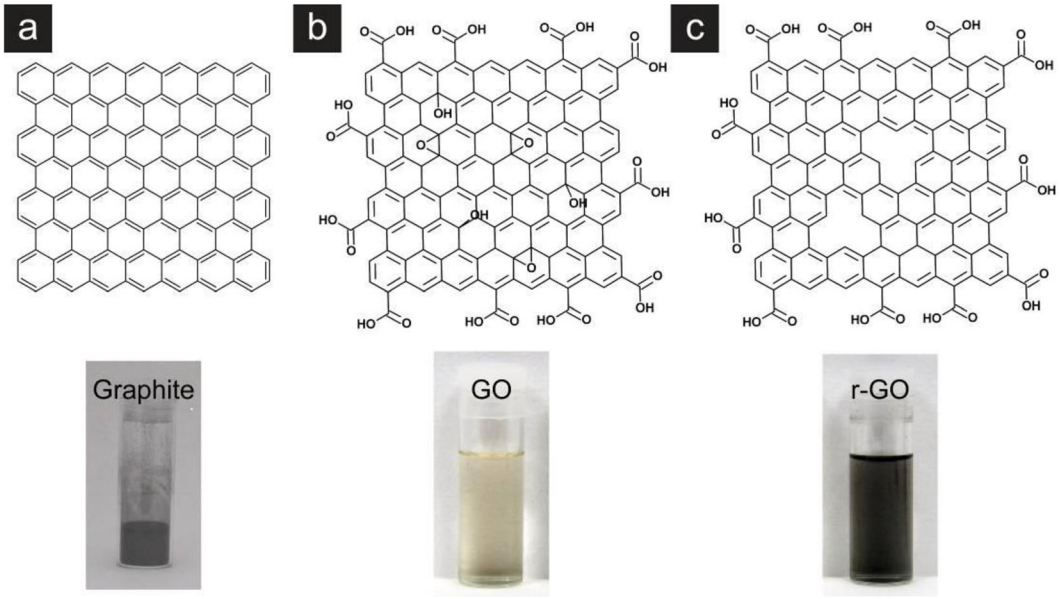

Fig. 1 Chemical structural models of graphene-based sheets. (a) Graphene consists of a single atomic layer of sp^2-hybridized carbon atoms which stack together to form graphite (below). (b) GO consists of a graphene sheet derivitized by phenyl epoxide and hydroxyl groups on the basal plane and carboxylic acid groups on the edges. The edge –COOH groups can ionize resulting in an electrostatic repulsion between the sheets, allowing single layers to form an aqueous colloidal dispersion (below). (c) Chemically modified graphene (r-GO), although more defective than graphene, has a partially restored π-conjugated network in its basal plane, resulting in a darker color in dispersion (below).

have been envisioned and demonstrated. Geim and Novoselov's groundbreaking discovery and experiments on graphene were recognized with the 2010 Nobel Prize in Physics.

Among the family of derivatized graphene sheets, graphite oxide sheets, now called graphene oxide (GO), have actually been made for over a century [4,5]. They are typically synthesized by reacting graphite powders (Fig. 1a) with strong oxidizing agents such as $KMnO_4$ in concentrated sulfuric acid. After oxidation, the graphene sheets are derivatized by carboxylic acid at the edges and phenol hydroxyl and epoxide groups mainly at the basal plane (Fig. 1b) [6,7]. Therefore, the sheets can readily be exfoliated to form a stable, light-brown-colored, single-layer suspension in water. This severe functionalization of the conjugated network renders GO sheets insulating. However, conductivity may be partially restored through reduction by chemical [8,9], thermal [10,11], photothermal [12,13], and photochemical [14] treatments, producing chemically modified graphene sheets (a.k.a., reduced GO, r-GO) (Fig. 1c). This oxidization-exfoliation-reduction cycle effectively makes the insoluble graphite powders processible in water, rendering many ways of using the conducting r-GO products. Although the resulting graphene product or r-GO is more defective and thus less conductive than pristine graphene, the ease of synthesizing GO and its solution processability has made it a very attractive precursor for graphene-based materials and devices, especially in large-scale production [15–17].

As shown in the three-dimensional structural model (Fig. 2a), a GO sheet is characterized by two abruptly different length scales. The thickness is of typical molecular dimensions, measured to be about 1 nm by atomic force microscopy (AFM) (Fig. 2b) [9,18]. But its lateral dimensions are of common colloidal particles, ranging from nanometers up to hundreds of microns. Therefore, GO sheets can be characterized as either molecules or particles, depending on which length scale/dimension is of greater interest. This molecule-particle duality should naturally make GO a particularly interesting system for

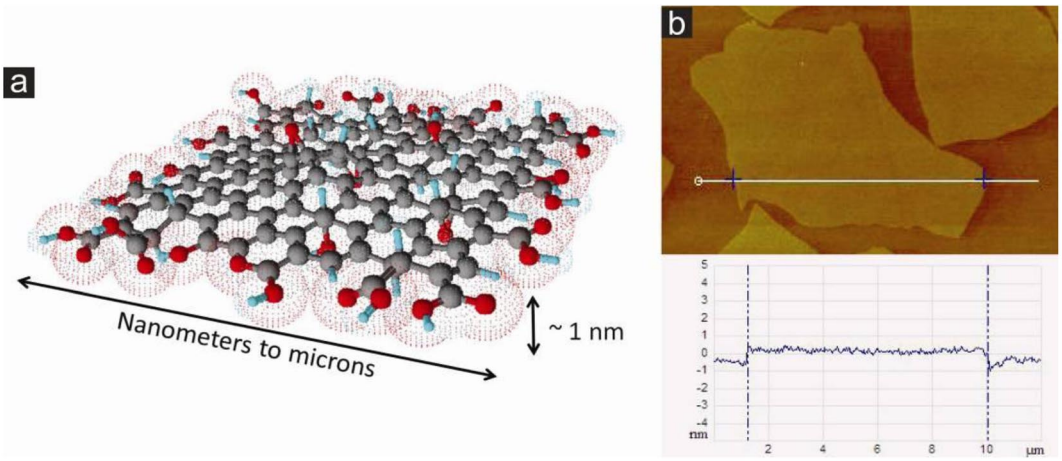

Fig. 2 Molecule-particle duality of GO. (a) Three-dimensional structural model and (b) an AFM image of GO sheets depicting two abruptly different length scales: The apparent thickness of the sheet is about 1 nm, a typical length scale of molecules, while its lateral dimension is of a length scale of common colloidal particles, ranging from nanometers to microns.

both chemists and material scientists. In this review, we would like to highlight an alternative perspective of GO sheets that views it as an unconventional soft material [19,20], such as an amphiphile, and present a few discoveries motivated by this fundamental scientific curiosity.

GO AS A NOVEL TWO-DIMENSIONAL AMPHIPHILE

Fundamental hypothesis

Since GO can easily disperse in water due to the ionizable edge –COOH groups, it has long been thought of as hydrophilic [16,21–24]. However, a closer look at its structure reveals that it may actually be amphiphilic. Although the edges of GO are hydrophilic (Fig. 3a, orange), its basal plane contains many polyaromatic islands of unoxidized graphene nanodomains (Fig. 3a, dark green). These hydrophobic, π-conjugated patches have recently been visualized directly by aberration corrected transmission electron microscopy (TEM) (Fig. 3b) [25]. Amphiphilic molecules contain both hydrophilic and hydrophobic regions, which are typically arranged in a linear, head-to-tail fashion. Such molecules are characterized by their ability to stabilize interfaces, or act as surfactants, for example, to form emulsions of oil and water or as dispersing agents to solubilize hydrophobic materials in water [26]. With the two-dimensional geometry of a GO sheet, many fundamental scientific questions arise about its surfactant behavior, including: Would GO act as a molecular or colloidal surfactant to stabilize interfaces? How will parameters such as size and degrees of functionalization affect the sheet's hydrophilic–hydrophobic balance and therefore interfacial activity? Would GO's edge-to-center configuration bring new surfactant functionalities? To answer these questions, we will first need to study GO's interfacial activities.

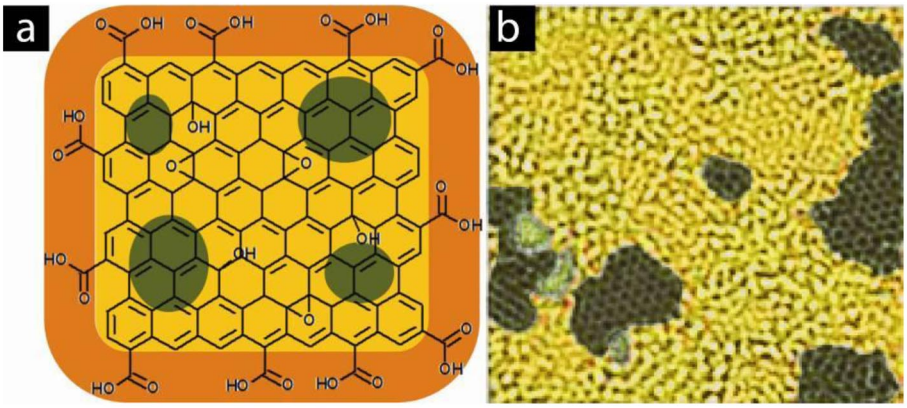

Fig. 3 GO as a surfactant sheet. (a) Structural model of GO depicting (orange) hydrophilic, ionizable edges and (dark green) hydrophobic, unoxidized graphitic nanopatches on the basal plane. (b) An aberration-corrected TEM image showing the nanographene islands (dark green) within the basal plane of a GO sheet (adapted from [25], with permission from Wiley-VCH).

Interfacial activity of GO

Molecular amphiphiles are compounds that can adhere to interfaces [26]. If GO is amphiphilic, it should also be surface active. Therefore, for an aqueous GO dispersion, GO sheets would adhere to the surface of water. Due to the large lateral dimension of GO, their presence at the air–water interface could be directly detected by Brewster angle microscopy (BAM). BAM is a surface-selective imaging technique in which *p*-polarized light is incident on the water surface at the Brewster angle, the angle at which no reflection is allowed (Fig. 4b, top). When a surface monolayer is introduced, the surface refractive index changes and thus allows reflection from that region (Fig. 4b, lower) [27]. However, initial BAM imaging of a freshly prepared GO dispersion revealed little material on the surface. This can be attributed to a slow diffusion process resulting from the sheet's large "molecular" mass. The journey to the air–water interface can be sped up by a flotation process, in which the surface active sheets adhere to rising gas bubbles and become trapped upon reaching the water surface (Fig. 4a). This was achieved with bubbling air or nitrogen through GO dispersion [28], alternatively commercial carbonated water can be used as a convenient in situ CO_2 source. This can be done by simply dispersing GO in carbonated water and subsequently adding boiling stones to release the dissolved gas. Indeed, flotation greatly enriches GO at the water surface, appearing as bright spots against a dark background in the BAM image (Fig. 4c) [29].

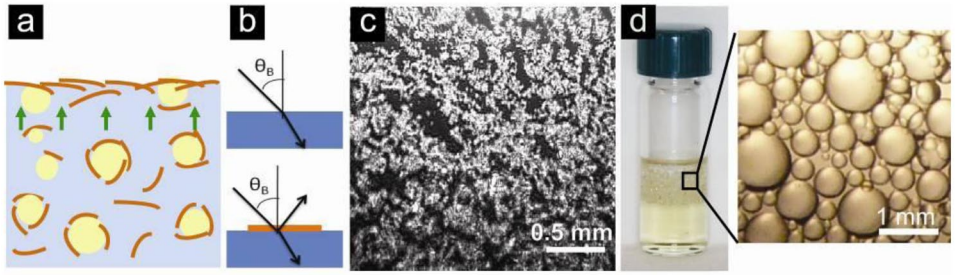

Fig. 4 Interfacial activity of GO. (a) GO can be enriched at water surface by flotation, appearing as white light-scattering spots in the (b,c) BAM images. (d) GO is also active at the oil–water interface, as it can stabilize Pickering emulsions of toluene in water (adapted from [29], with permission from ACS Publications).

With their colloidal particle nature, GO sheets were also found to be capable of stabilizing oil–water interfaces to form the particle-stabilized Pickering emulsions [30]. As shown in Fig. 4d, gentle shaking of a toluene/GO water biphasic mixture results in large toluene droplets in water (Fig. 4d). These large droplets can remain kinetically stable for many months since GO sheets are now trapped at the oil–water interfaces [29]. Drop formation was found to occur more readily with aromatic solvents, like toluene and benzene, than with nonaromatic solvents, such as chloroform and hexane, indicating π–π interactions between the solvent and GO's basal plane contribute to emulsion stability. As with other particle-stabilized emulsions, the droplet size was found to depend on colloidal concentration, with droplet size increasing as concentration decreases.

Tunable amphiphilicity of GO sheets

Being a sheet-like surfactant, GO's amphiphilicity originates from the hydrophilic edges and hydrophobic groups in its basal plane. For example, like ionic molecular surfactants, its amphiphilicity would vary with the degree of ionization of the edge –COOH groups, or the pH of the dispersion (Fig. 5a). Higher pH values would result in increased edge charges and therefore increased hydrophilicity of the sheet. GO's edge-to-center arrangement of hydrophilic and hydrophobic groups suggests that size should be a tuning parameter, too. It would be expected that smaller sheets, with a higher edge-to-area ratio, are more hydrophilic (Fig. 5b). Lastly, the size of hydrophobic nanographene regions on the basal plane of the GO sheet could be tuned by different degrees of reduction, or removal of oxygen functionalities (Fig. 5c) from the sheets [25]. An initial verification of these hypotheses can be made by studying the effects of pH, size, and degree of reduction on the charge density and therefore hydrophilicity of GO. As shown in the zeta potential measurements (Fig. 5d), the charge density of GO sheets indeed decreases with decreasing pH values, increased sheet sizes, and increased degree of reduction.

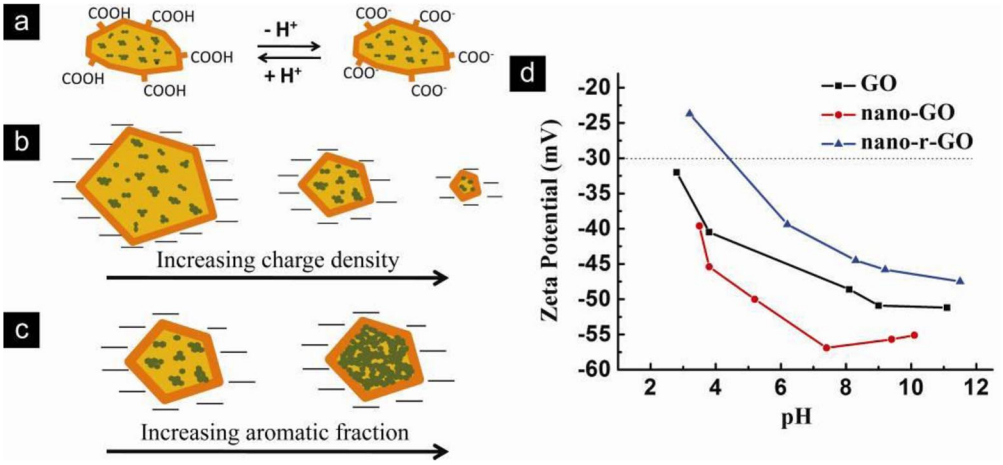

Fig. 5 Amphiphilicity of GO is dependent on pH, sheet size, and degree of reduction as shown schematically in a, b, and c, respectively. (d) Zeta potential measurements show the charge density (i.e., hydrophilicity) of GO increases with higher pH, smaller size (from regular micron-sized GO to nano-GO with diameter <100 nm) and lower degree of reduction (nano-r-GO to nano-GO).

IMPACTS AND APPLICATIONS

Two-dimensional assembly of GO sheets on air–water interface

Amphiphilicity is a fundamental solution property of materials. The new insight that GO is amphiphilic should lead to a better understanding of the processing and assembly of GO sheets. GO can be solution-processed to form thin films by many techniques such as spin coating, drop casting, spraying, and dip coating, etc. [15,17]. However, precise control over film thickness (i.e., number of layers) is difficult in these techniques. Since GO is a surfactant, we can now take advantage of its surface activity and employ the classical molecular assembly methods, such as the Langmuir–Blodgett (LB) technique [31] to create monolayers. In the classical LB technique, a surfactant monolayer is spread on the water surface and confined between two movable barriers (Fig. 6a) [31]. As the barriers are closed, the surface density of molecules increases, leading to an increase in surface pressure, or reduction in surface tension that can be continuously monitored by a tensiometer. The floating monolayers can then be transferred to a solid support by vertical dip-coating. This technique has also been used to prepare monolayers of polymers and nanomaterials [32]. The two-dimensional water surface should serve as an ideal platform to assemble GO sheets. First, the interface is geometrically similar to GO, making it ideal to accommodate the flat sheets. Second, the soft, fluidic "substrate" should allow free movement of GO sheets upon manipulation. Third, water surface tension can help to keep the soft sheets flat, free from wrinkling or crumpling.

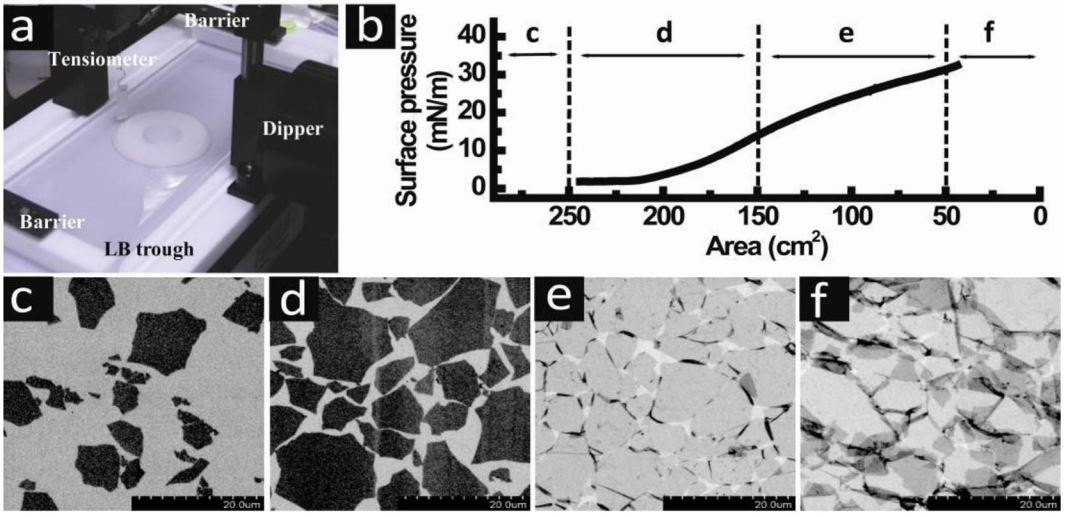

Fig. 6 LB assembly of GO sheets. (a) With an LB trough, the surface density of GO sheets can be continuously manipulated by the barriers, and the surface pressure can be monitored by the tensiometer. Monolayers can be transferred to a solid substrate by dip-coating. (b) Surface pressure-area isotherm of a GO monolayer showing a continuously increasing surface pressure with decreasing area. (c–f) SEM images of monolayers collected from the corresponding regions in the isotherm plot, showing continuously tunable surface coverage from (c) isolated flat sheets, (d) close-packed sheets, (e) overpacked sheets with folded edges to (f) overpacked sheets interlocked with each other (adapted from [18], with permission from ACS Publications).

Though typical spreading solvents are volatile and water-immiscible (e.g., chloroform, toluene), these solvents do not disperse GO well [22]. Since GO is amphiphilic, it can be spread from alcohols that are even miscible with water, such as methanol [18]. When methanol droplets are gently dropped on water surface, it can first spread rapidly on the surface before mixing with water. In this way, the GO

surfactant sheets can be effectively trapped at the air–water interface. The density of sheets can then be continuously tuned by moving the barriers. Upon compression, the monolayer exhibits a gradual increase in surface pressure, as shown in the surface-pressure–area isotherm plot (Fig. 6b). Films collected by dip-coating along the compression curve were imaged by scanning electron microscopy (SEM) and showed four distinct packing behaviors. At the initial stage where the surface pressure is near zero, the collected film consists of dilute, well-isolated flat sheets (Fig. 6c). As compression continues, a gradual increase in surface pressure begins to occur and the sheets start to close pack into a broken tile mosaic pattern over the entire surface (Fig. 6d). Upon further compression, the soft sheets are forced to fold and wrinkle at their touching points in order to accommodate the increased pressure (Fig. 6e). This is in stark contrast to traditional molecular or colloidal monolayers which would collapse into double layers resulting in a constant or decreasing surface pressure when compressed beyond the close-packed regime [33]. Even further compression resulted in interlocked sheets with nearly complete surface coverage (Fig. 6f). The LB assembly produces flat GO thin films with uniform and continuously tunable coverage, thus avoiding the uncontrollable wrinkles, overlaps, and voids in films fabricated by other techniques [15].

Establishing structure–property relationship of r-GO monolayers

The monolayer shown in Fig. 6f has continuous and dense surface coverage. Upon reduction, it can turn into a conductive r-GO thin film. The properties of the resulting monolayer depend not only on the quality of the individual sheets but also on how they are assembled, which generates thin film microstructures that ultimately determine the film properties. Therefore, LB monolayers can be used as a model system to investigate such microstructure–property relationships of solution-processed graphene-based thin films. For example, wrinkles and overlaps are the two fundamental morphologies between flexible, interacting sheets that are usually convoluted in solution-processed GO thin films. If these two types of features can be individually produced, we will be able to deconvolute how these two basic microstructures affect the electrical and optical properties of the final thin films.

The surfactant-like properties of GO sheets suggest that one could potentially control how they assemble at the air–water interface by tuning their amphiphilicity. Since the dissociation of edge –COOH groups is pH-dependent, the edge-to-edge interaction between GO sheets should also be pH-dependent [29]. This can be conveniently studied by adjusting the pH values of the water subphase during LB assembly. As shown in Figs. 7a,b, in situ BAM images reveal a clear change in GO packing on the water surface when the subphase pH is increased from acidic (pH 5.5) to basic (pH 10) levels [34]. On an acidic subphase, the initial monolayer has many islands of aggregated GO pieces (Fig. 7a), which are forced to arrange together as the monolayer is further compressed. When the subphase pH is raised, these islands disappear and the monolayer appears more uniform as GO sheets experience greater electrostatic repulsion (Fig. 7b). This change in aggregation state is accompanied by a drastic change in the final surface pressure for compressed films, with a decrease typically from around 25 mN/m in acidic subphase to a few mN/m in basic subphase. The large surface pressure drop indicates a change in the microstructure of the monolayer, of which the interacting GO sheets may adopt a less-strained configuration.

To investigate this, we collected monolayers in a highly compressed state from both acidic and basic conditions to achieve high surface coverage. The samples are thus termed “acidic” and “basic” monolayers, respectively. Three microscopy techniques were used, namely, fluorescence quenching microscopy (FQM) [35,36], SEM [18,36], and AFM to image the samples at length scales from millimeter down to submicron. Large-area overview images collected by FQM (Figs. 7c,d) show comparable coverage for both monolayers. However, parallel wrinkles are seen in the acidic monolayer as depicted by the darker lines. The wrinkles are perpendicular to the direction of compression, indicating the entire monolayer buckled as one under compression. A more detailed view by SEM (Fig. 7e) reveals many smaller wrinkles on the individual sheets. Such wrinkles typically occur near the edges of the GO

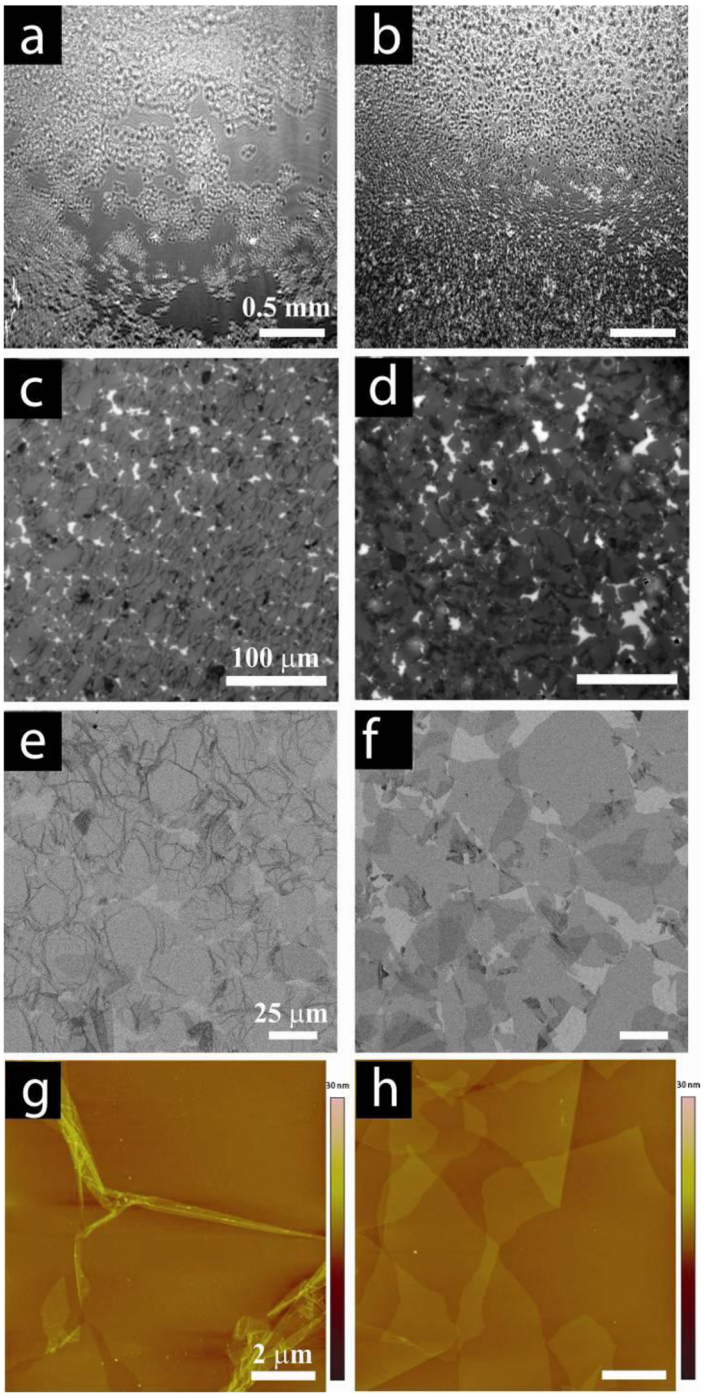

Fig. 7 pH-dependent LB assembly of GO sheets observed by (a,b) BAM, (c,d) FQM, (e,f) SEM, and (g,h) AFM. At mild compressions, (a) sheets in the acidic monolayer form islands, while (b) in basic monolayer the sheets disperse more evenly. In the fully compressed state, wrinkles (c,e,g) and overlaps (d,f,h) are the dominating microstructures in acidic and basic monolayers, respectively (adapted from [34], with permission from The Royal Society of Chemistry).

sheet and are aligned to the contact lines of the interacting sheets, suggesting that they are also buckling structures developed under in-plane compressive stress. AFM images (Fig. 7g) on individual wrinkled sites show that they are typically more than 3 nm high and often reach 5–10 nm, effectively creating many 5–10-layer islands in the 1-nm-thick monolayer. In contrast, few wrinkles are seen in the basic monolayers, whose microstructures are dominated by partial overlaps between neighboring sheets (Figs. 7d,f,h). The different packing behaviors are attributed to the pH-dependent hydrophilicity of GO sheets. GO sheets are more hydrophilic and wettable by water in basic conditions. Therefore, they could acquire a water lubrication layer, allowing them to slide on each other, thus avoiding compressing each other under compression. Overlapping also helps to reduce electrostatic repulsion between the charged edges of GO sheets. Under acidic conditions, the sheets are more hydrophobic and would be forced to squeeze each other upon compression. Hydrogen bonding between the protonated edge carboxylic acid groups and water surface tension may also prevent the sheets from sliding, forcing wrinkles to form during compression. Indeed, the wrinkled microstructures require higher surface pressure to maintain compared with the overlapped state, accounting for the above-mentioned drop in surface pressure when the subphase is tuned from acidic to basic conditions.

Wrinkles and overlaps are common features in GO and graphene thin films. pH-dependent LB assembly can now offer model systems to deconvolute the effects of these two types of microstructures on thin film properties, thus establishing a well-defined structure–property relationship [34]. As a proof of concept, we examined the effect of wrinkles and overlaps on the film's sheet resistance and optical transmission, the two most important performance parameters for transparent conductor thin films [37–41]. The sheet resistance of the r-GO monolayers, which were thermally reduced at 500 °C in Ar was measured between patterned gold electrodes with a narrow width of 0.25 mm and wide width of 2.5 mm (Fig. 8a). The distribution of sheet resistance values measured at different spots on the film directly reflects the uniformity of coverage of the r-GO film. Uniform coverage should result in consistent sheet resistance measurements, insensitive to electrode separation. Otherwise, the apparent values would scatter, especially with narrower electrode gaps. Sheet resistance values measured on the acidic, wrinkled monolayer (Fig. 8a, solid and hollow squares) have wide distributions, especially for those measured with a narrow gap width (solid black squares), which scatter nearly two orders of magnitude. Conversely, values measured on the basic, overlapped monolayer (Fig. 8a, solid and open circles) are much more consistent, regardless of electrode separation. FQM images of the thin films reveal that the wider distributions in wrinkled films are indeed due to less uniform coverage. This is consistent with the BAM observations over a large area (Figs. 7a,b). Overall, the sheet resistance values for acidic monolayers were only slightly higher but are more scattered than those of the basic monolayers.

These morphological features also affect the optical properties of the thin films. As shown in the AFM images (Figs. 8b,c), the wrinkled sites are much rougher than the overlapped ones. Therefore, they can scatter light strongly, causing higher optical loss, thus decreasing the transparency of the monolayer. For example, the average percent transmission of the r-GO monolayers shown in Fig. 8 with wrinkles and overlaps was measured to be 94.1 and 96.1 %, respectively. This effect can be directly imaged with a dark field optical microscope. As shown schematically in Figs. 8 d,e, in dark field imaging mode, light is incident on the sample at an oblique angle, such that only light scattered by the sample can enter the front lens to form an image. The bright wrinkles can be clearly seen against the black background (Fig. 8d), while the overlaps are essentially featureless. An aggregation of GO was shown in Fig. 8e only to focus the camera for the overlapped sample.

The greater roughness of wrinkled r-GO film is also a disadvantage for organic thin film device applications since these pointy sites have higher probability to generate short circuit. Although the structure–property relationship described here was established with LB assembly of tiled GO pieces, the knowledge gained here should be useful for graphene films made by other methods. For example, graphene thin films made by chemical vapor deposition also start from isolated small domains, which

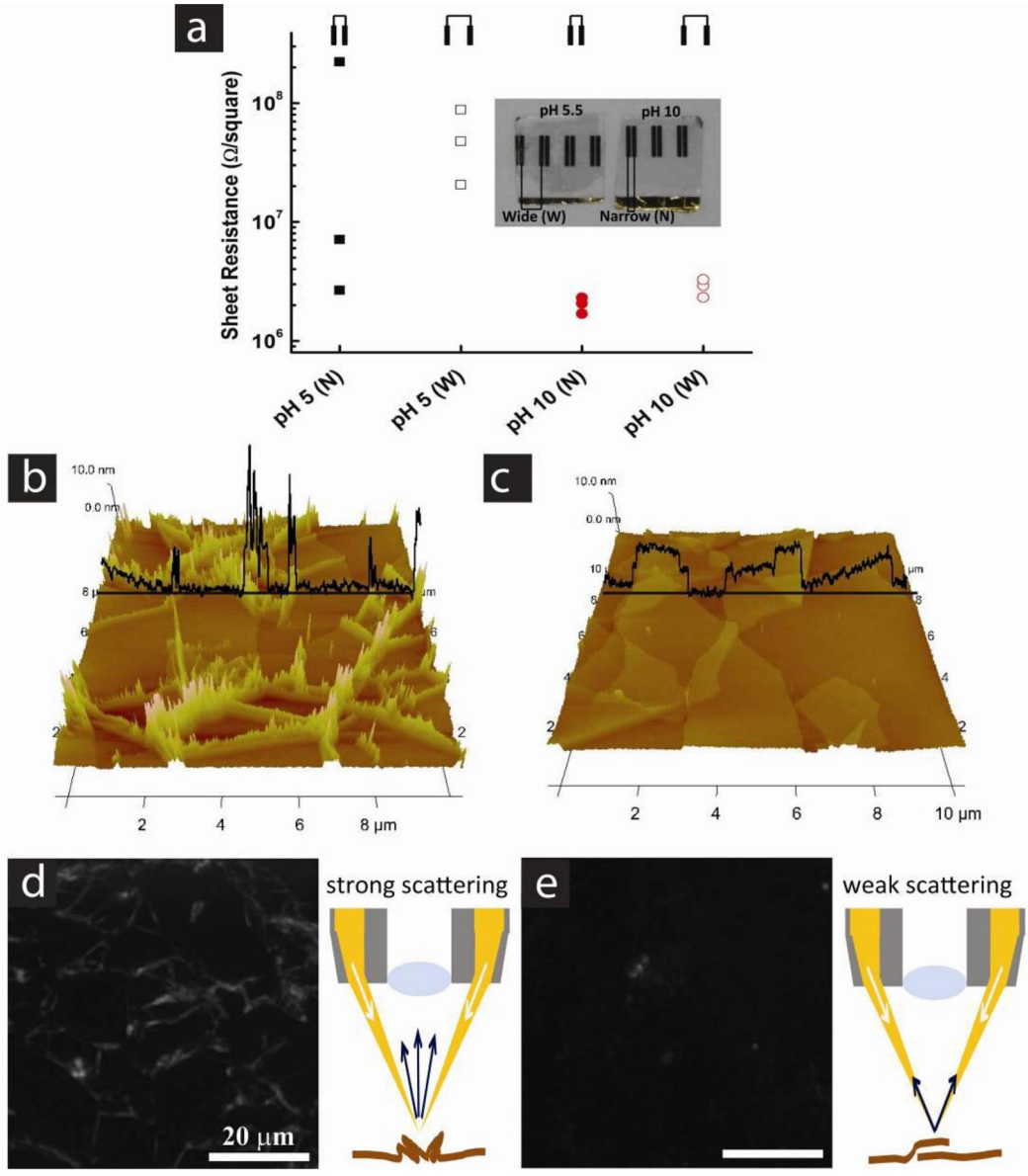

Fig. 8 Wrinkles and overlaps: Structure–property relationship of r-GO monolayers. (a) Sheet resistance of the "wrinkled" r-GO monolayer (black squares) scatter greatly, indicating a lower film uniformity compared to that of the "overlapped" monolayer (red circles). Inset shows samples with gold electrodes of wide (2.5 mm) and narrow (0.25 mm) separations. (b,c) Three-dimensional view and line scan over the black line of AFM images showing much greater surface roughness of the wrinkled films compared with that of the overlapped film. (d,e) Dark field optical microscopy images of wrinkled and overlapped samples, respectively. Wrinkles can be directly imaged (d) due to strong scattering, which causes higher optical loss of the monolayer. The overlapped monolayer is essentially featureless, suggesting much weaker optical scattering (adapted from [34], with permission from The Royal Society of Chemistry).

grow larger and merge to achieve complete coverage of the substrate. Therefore, wrinkles and overlaps are also common features between the neighboring domains [42].

Size separation of GO

During the synthesis and processing of GO, the graphene sheets in the graphite particles are not only derivatized with oxygen-containing groups but also torn up into smaller pieces. As a result, the lateral sizes of the as-synthesized GO sheets are usually very polydisperse, ranging from a few nanometers to tens of micrometers, which may even vary from synthesis to synthesis. Based on their size-dependent amphiphilicity (Fig. 5b), new size separation techniques can be envisioned for GO. To test this, we mixed small sheets (<1 μm) made by heavily sonicating a GO dispersion with unsonicated large sheets (>5 μm) (Fig. 9a). This stock dispersion was spread onto the water surface in an LB trough (Fig. 9b). Samples were collected by dip-coating from the surface between the LB trough's barriers, (Fig. 9c) and from the subphase outside the barriers (Fig. 9d). SEM images of the collected samples (Figs. 9c,d) clearly show a spontaneous size separation on the water surface. Large, less hydrophilic sheets can float on the water surface while small, more hydrophilic sheets sink into the subphase. Therefore, the water surface itself, without any features, can be used as a size-separation filter for GO sheets [29]!

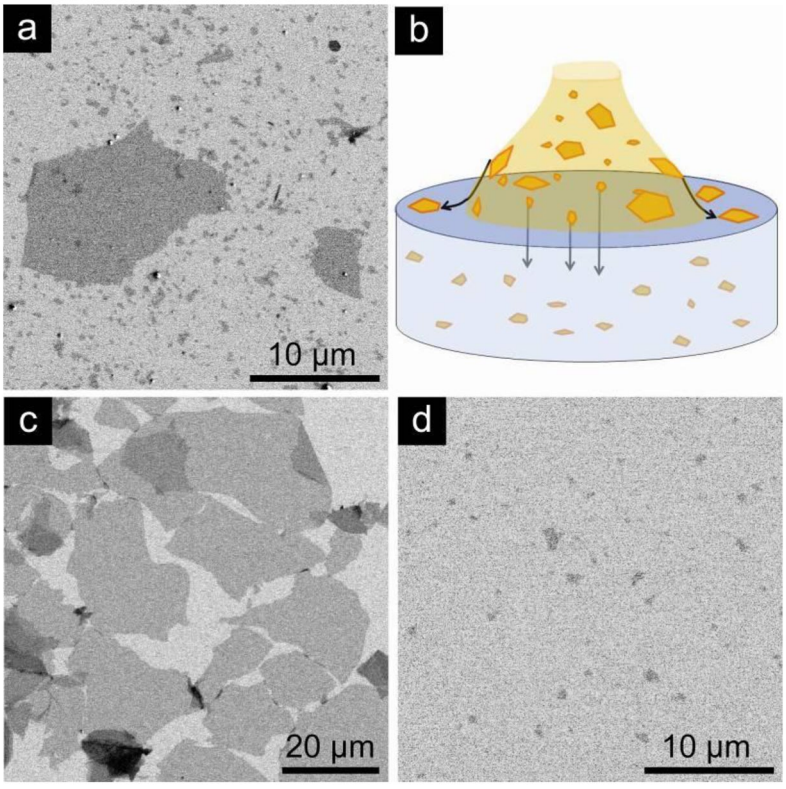

Fig. 9 Size separation of GO using the water surface as a filter membrane. (a) SEM image of GO sheets drop cast from a dispersion containing both large (>5 μm) and small (<1 μm) sheets. (b) When spread on water surface, the smaller, more hydrophilic sheets sink into the subphase, while the larger, more hydrophobic sheets stay trapped on water surface as shown in the SEM images of samples collected from (c) water surface and (d) the subphase, respectively (adapted from [29], with permission from ACS Publications).

Size-dependent amphiphilicity of GO is also reflected by their emulsifying power, which in turn can be utilized to do size separation. A proof-of-concept experiment is shown in Fig. 10b. Toluene is added to a GO dispersion and shaken to form Pickering emulsions. The emulsions effectively extracted

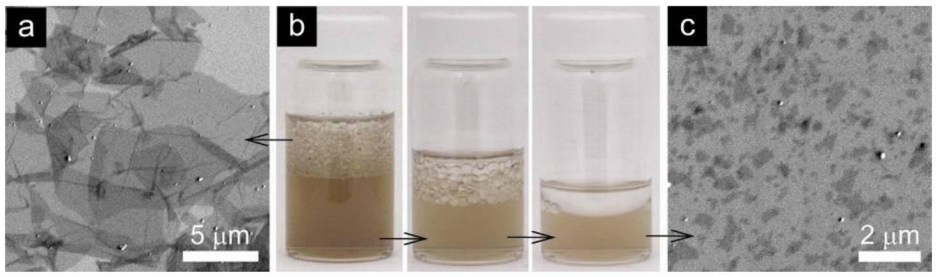

Fig. 10 Size separation of GO sheets by emulsion extraction. GO's size-dependent amphiphilicity is reflected in their emulsifying capability. As organic solvent (e.g., toluene) is added to GO dispersion to form emulsions (b), it extracts a portion of GO sheets from water, which are found to be mainly large sheets (>5 μm) as shown in the SEM image (a). Sequential emulsion extraction steps (b) would eventually deplete the large sheets, leaving the small sheets (<1 μm) that are not capable of emulsifying toluene in the water as shown in the SEM image (c).

a portion of GO sheets from the aqueous phase. Then the remaining GO dispersion can be drained and subjected to a few more extraction steps by toluene, until no more emulsions can be produced. SEM images show that the sheets collected from the emulsion phase (Fig. 10a) are large sheets (>5 μm). As the large sheets are continually removed in sequential extraction steps, the final portion of GO sheets left in water are much smaller ones (<1 μm) that are (Fig. 10c) not capable of stabilizing the emulsion droplets. The extracted large sheets can be redispersed in water by solvent exchange, adjusting pH, or directly depositing on substrates by dip-coating.

GO as dispersing agent

One major use of surfactants is as a dispersing agent for the solution processing of insoluble solids. The surfactant behavior of GO at the air–water and oil–water interfaces suggests that GO may also act as a dispersing agent to stabilize the solid–liquid interface. Unlike small molecular surfactants, a GO sheet has much larger lateral dimension and an array of hydrophobic, π-conjugated nanopatches in the basal plane. This allows GO to adhere to or even wrap an insoluble particle with multiple adhesion sites, much like octopi capturing their prey with suction cups. As a proof of concept, graphite and carbon nanotubes (CNTs) are used as a model system since they are both known to be difficult to disperse in water and could have π–π interactions with π patches on GO's basal plane [29]. Figure 11a shows that graphite powders are not capable of being dispersed in water even after sonication, however, with the addition of GO, the materials are effectively dispersed and stay stable for days. SEM images of the graphite powders after being sonicated in water reveal large platelets of tens of microns (Fig. 11b), however, in the presence of GO, much smaller particles with diameters of only a few microns (Fig. 11c) are produced. The greater size reduction in GO dispersion suggests that graphite powders are more effectively sonicated. It is likely a result of surface functionalization of graphite by GO, making the particles better suspended, thus better sonicated. In addition, the presence of GO in the solution should impede the motion of graphite particles during sonication, resulting in a larger fraction of the sonication energy being transferred to break up the particles.

Figure 11d shows that CNTs can also be dispersed by sonication in a GO dispersion, creating a colloidal dispersion stable for at least several months. In contrast, sonication in pure water is ineffective. SEM images of the water-sonicated CNT reveal heavily entangled tubes (Fig. 11e) which are disentangled by sonication in GO dispersion (Fig. 11f). Microscopy analysis reveals that almost all of the CNTs are disentangled and adhere to GO. Unlike typical dispersing agents for CNTs such as molecular surfactants [43,44], polymers [45], and DNA [46], GO can be readily reduced to chemically modified graphene, which makes GO a functional surfactant for solution processing. GO was also found to

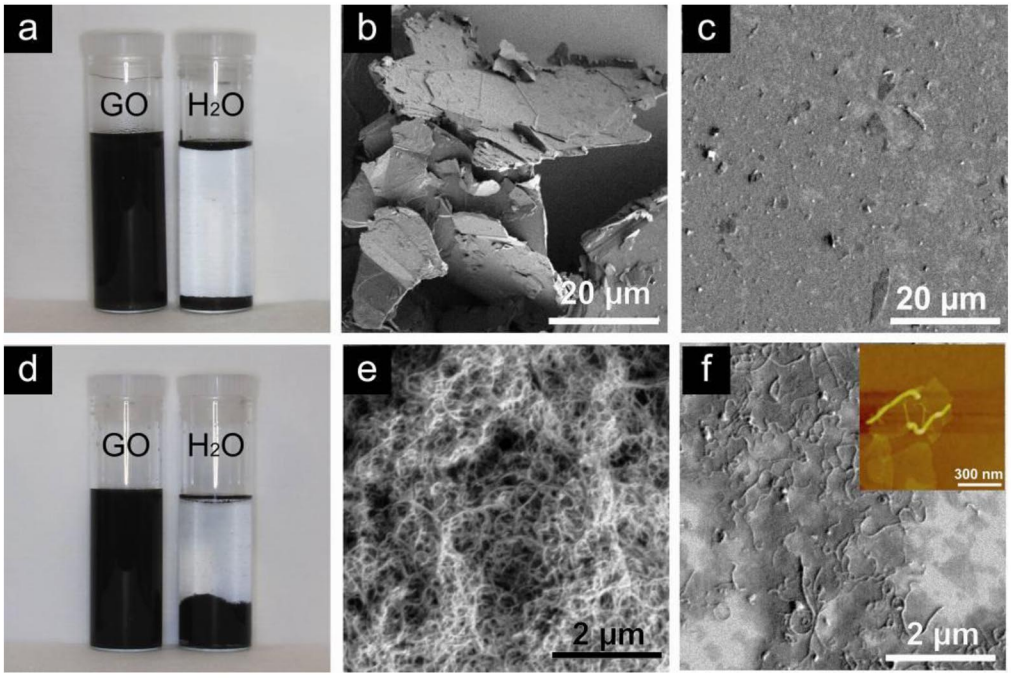

Fig. 11 GO acts as a surfactant to disperse insoluble materials in water. (a) Graphite powder and (d) CNTs are stabilized by a GO dispersion after sonication (left vials). In contrast, sonication does not disperse the materials in pure water (right vials). (c) Sonication of graphite in GO dispersion result in orders of magnitude size reduction compared with (b) sonication in water as shown in the SEM images. (e) Sonication of CNTs in water cannot break the entangled bundles, while (f) sonication of CNTs in a GO dispersion disentangles the tubes. (f, inset) AFM image shows that the CNTs are adhered to the GO surfactant sheets (adapted from [29], with permission from ACS Publications).

be capable of dispersing other π-conjugated materials such as organic semiconductors and conducting polymers.

All-carbon composites

CNTs and graphene-based sheets have long been touted as promising materials for energy storage such as in ultracapacitors due to their high electrical conductivity and surface area [47]. However, when used individually, both CNTs and graphene are prone to aggregation that will greatly limit their accessible surface area, which prevents the full realization of their high specific capacitance. This problem can be solved by co-assembling these two geometries—sheets and tubes—to form CNTs-intercalated graphene stacks. Typically, the assembling strategies involve functionalizing CNT and/or graphene or r-GO sheets with dispersing agents [48,49] before mixing, which could introduce hard-to-remove impurities into the final composites. Direct mixing was also achieved using highly unstable and highly toxic solvents such as anhydrous hydrazine [50]. The new insight of GO's amphiphilicity provides an immediate solution since CNT-intercalated graphene films can now be easily made by sonicating unfunctionalized CNTs in GO water, followed by thermal or chemical reduction. As shown in Fig 12, the CNTs enveloped in between adjacent GO layers serve as both spacer to prevent restacking of the sheets, and as additional electrical conduction paths to improve the overall conductivity. The CNTs/GO hybrid can be transformed to a conductive, all-carbon composite using either thermal or chemical reduction. Note that the reduction of GO does not generate any hard-to-remove byproduct, thus enabling good car-

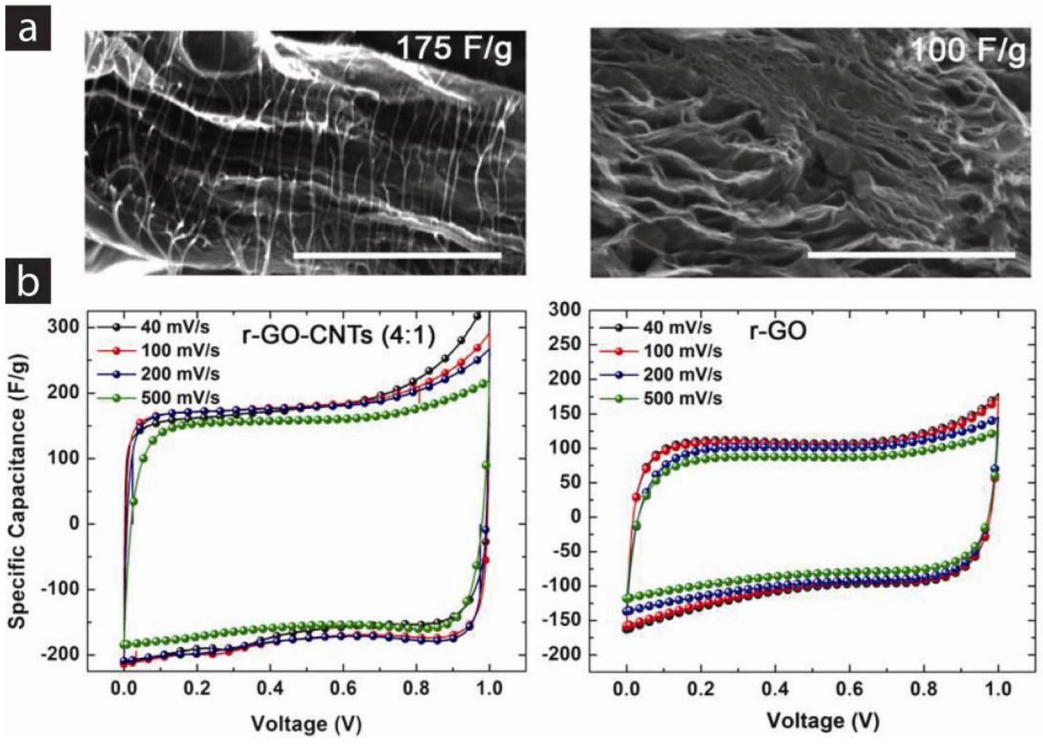

Fig. 12 An all-carbon composite of CNTs/r-GO with enhanced electrochemical double-layer ultracapacitor performance. (a) High-resolution cross-sectional SEM images of CNTs/r-GO (left) and r-GO (right) films. Scale bars = 500 nm. (b) Specific capacitance of CNTs/r-GO and r-GO electrodes under different scan rate. Note that CNTs/r-GO composite displays higher specific capacitance and more stable power delivery at faster scan rate up to 500 mV/s.

bon–carbon interconnect in the composite. Thermal and chemical reduction also lead to gas evolution from GO, ultimately forming slightly expanded structures, in which the horizontal CNTs are now stretched along the normal direction to the sheets, forming pillars to support the hybrid structure as shown in the cross-sectional SEM images (Fig. 12a, left). The resulting all-carbon hybrid was used as electrode material for electrochemical double-layer ultracapacitors. Cyclic voltammetry measurements (Fig. 12b) show that after incorporating CNTs, the specific capacitance of r-GO film increase from 100 to 175 F/g at a scan rate of 40 mV/s due to more accessible surface area by the electrolyte. Meanwhile, the shape of the cyclic voltammetry curves of the hybrid is more rectangular than that of the r-GO, and the specific capacitance of the hybrid is also more stable as the voltage scan rate changes due to higher internal conductance of the electrode material allowing more efficient charge propagation. As shown in Fig 12b, when the scan rate increases from 40, 100, 200, to 500 mV/s, the specific capacitance of CNTs/r-GO only decreased by 2–5 %, while for r-GO electrode, it decreased by 10 %. Using GO as a surfactant eliminates the need for expensive and laborious material preparation methods. It will open up the possibility of preparing many other all-carbon or carbon-rich materials.

CONCLUSIONS

Despite being considered hydrophilic for the past century, GO is a unique two-dimensional amphiphile that can adhere to gas–water, liquid–water, and solid–water interfaces and lower interfacial energy [29]. Its amphiphilicity is tunable by solution pH values, sheet size, and degree of reduction. This new insight

allows better understanding of the solution property of GO, which is helpful for designing better assembly and processing techniques for graphene thin films [18,28]. Well-defined microstructure–property relationship of graphene monolayers can be established by tuning the assembly of these surfactant sheets [34]. Size-dependent amphiphilicity inspires novel size separation methods such as water surface filtration and emulsion extraction. GO sheets can be used as dispersing agents to create colloidal dispersions of insoluble materials, especially π-conjugated aromatic systems such as conjugated polymers, CNTs, and graphite, thus enabling their solution processability. As a novel surfactant, GO offers a few advantages. For example, as a colloidal surfactant with large dimension, they can be easily recovered (e.g., by filtration). They can be readily converted to chemically modified graphene, rendering the final complex of surfactant-dispersed phase electrically conductive. When GO is used to disperse carbon-based materials, it allows for the creation of clean carbon–carbon junctions that would otherwise be contaminated by common molecular surfactants or degraded by covalent functionalization, which should facilitate charge transport across the interfaces. Since surfactants are routinely used in chemical and material industries as well as in our daily life, perhaps what this new surfactant system can do is only limited by our imagination.

ACKNOWLEDGMENTS

This work was primarily supported by the National Science Foundation (CAREER DMR 0955612). Additional supports were provided by the Initiative for Sustainability and Energy at Northwestern (ISEN), the Northwestern Nanoscale Science and Engineering Center (NSF EEC 0647560), the Northwestern Materials Research Science and Engineering Center (NSF DMR-0520513) and the Sony Corporation. L.J.C. is a NSF graduate research fellow. We thank Y. Wa, Prof. K. R. Shull, Z. Zhang, J. H. Huang, Prof. C. W. Chu, and Prof. C. Sun for collaboration in some of the works presented in this review.

REFERENCES

1. E. Fitzer, K. H. Kochling, H. P. Boehm, H. Marsh. *Pure Appl. Chem.* **67**, 473 (1995).
2. K. S. Novoselov, A. K. Geim, S. V. Morozov, D. Jiang, Y. Zhang, S. V. Dubonos, I. V. Grigorieva, A. A. Firsov. *Science* **306**, 666 (2004).
3. A. K. Geim, K. S. Novoselov. *Nat. Mater.* **6**, 183 (2007).
4. B. C. Brodie. *Philos. Trans. R. Soc. London* **149**, 249 (1859).
5. W. S. Hummers, R. E. Offeman. *J. Am. Chem. Soc.* **80**, 1339 (1958).
6. A. Lerf, H. Y. He, M. Forster, J. Klinowski. *J. Phys. Chem. B* **102**, 4477 (1998).
7. W. Gao, L. B. Alemany, L. Ci, P. M. Ajayan. *Nat. Chem.* **1**, 403 (2009).
8. W. H. Dobelle, M. Beer. *J. Cell Biol.* **39**, 733 (1968).
9. S. Stankovich, D. A. Dikin, R. D. Piner, K. A. Kohlhaas, A. Kleinhammes, Y. Jia, Y. Wu, S. T. Nguyen, R. S. Ruoff. *Carbon* **45**, 1558 (2007).
10. R. C. Croft. *Quarterly Rev.* **14**, 1 (1960).
11. H. C. Schniepp, J. L. Li, M. J. McAllister, H. Sai, M. Herrera-Alonso, D. H. Adamson, R. K. Prud'homme, R. Car, D. A. Saville, I. A. Aksay. *J. Phys. Chem. B* **110**, 8535 (2006).
12. L. J. Cote, R. Cruz-Silva, J. Huang. *J. Am. Chem. Soc.* **131**, 11027 (2009).
13. S. Gilje, S. Dubin, A. Badakhshan, J. Farrar, S. A. Danczyk, R. B. Kaner. *Adv. Mater.* **22**, 419 (2010).
14. G. Williams, B. Seger, P. V. Kamat. *ACS Nano* **2**, 1487 (2008).
15. M. J. Allen, V. C. Tung, R. B. Kaner. *Chem. Rev.* **110**, 132 (2010).
16. S. Park, R. S. Ruoff. *Nat. Nanotechnol.* **4**, 217 (2009).
17. O. C. Compton, S. T. Nguyen. *Small* **6**, 711 (2010).
18. L. J. Cote, F. Kim, J. Huang. *J. Am. Chem. Soc.* **131**, 1043 (2009).

19. I. W. Hamley. *Introduction to Soft Matter: Polymers, Colloids, Amphiphiles and Liquid Crystals*, John Wiley, New York (2007).
20. R. A. L. Jones. *Soft Condensed Matter*, Oxford University Press (2002).
21. D. A. Dikin, S. Stankovich, E. J. Zimney, R. D. Piner, G. H. B. Dommett, G. Evmenenko, S. T. Nguyen, R. S. Ruoff. *Nature* **448**, 457 (2007).
22. S. Gilje, S. Han, M. Wang, K. L. Wang, R. B. Kaner. *Nano Lett.* **7**, 3394 (2007).
23. D. Li, R. B. Kaner. *Science* **320**, 1170 (2008).
24. D. Li, M. B. Muller, S. Gilje, R. B. Kaner, G. G. Wallace. *Nat. Nanotechnol.* **3**, 101 (2008).
25. K. Erickson, R. Erni, Z. Lee, N. Alem, W. Gannett, A. Zettl. *Adv. Mater.* **22**, 4467 (2010).
26. D. Myers. *Surfactant Science and Technology*, Wiley-Interscience, Hoboken, NJ (2006).
27. M. M. Lipp, K. Y. C. Lee, J. A. Zasadzinski, A. J. Waring. *Rev. Sci. Instrum.* **68**, 2574 (1997).
28. F. Kim, L. J. Cote, J. Huang. *Adv. Mater.* **22**, 1954 (2010).
29. J. Kim, L. J. Cote, F. Kim, W. Yuan, K. R. Shull, J. Huang. *J. Am. Chem. Soc.* **132**, 8180 (2010).
30. S. U. Pickering. *J. Chem. Soc.* **91**, 2001 (1907).
31. M. C. Petty. *Langmuir-Blodgett Films: An Introduction*, Cambridge University Press, Cambridge, UK (1996).
32. A. R. Tao, J. X. Huang, P. D. Yang. *Acc. Chem. Res.* **41**, 1662 (2008).
33. C. Ybert, W. X. Lu, G. Moller, C. M. Knobler. *J. Phys. Chem. B* **106**, 2004 (2002).
34. L. J. Cote, J. Kim, Z. Zhang, C. Sun, J. Huang. *Soft Matter* (2010). doi: 10.1039/C1030SM00667J
35. J. Kim, L. J. Cote, F. Kim, J. Huang. *J. Am. Chem. Soc.* **132**, 260 (2010).
36. J. Kim, F. Kim, J. Huang. *Materials Today* **13**, 28 (2010).
37. H. c. A. Becerril, J. Mao, Z. Liu, R. M. Stoltenberg, Z. Bao, Y. Chen. *ACS Nano* **2**, 463 (2008).
38. S. De, J. N. Coleman. *ACS Nano* **4**, 2713 (2010).
39. G. Eda, G. Fanchini, M. Chhowalla. *Nat. Nanotechnol.* **3**, 270 (2008).
40. Q. Su, S. P. Pang, V. Alijani, C. Li, X. L. Feng, K. Mullen. *Adv. Mater.* **21**, 3191 (2009).
41. X. Wang, L. Zhi, K. Mullen. *Nano Lett.* **8**, 323 (2007).
42. X. S. Li, W. W. Cai, L. Colombo, R. S. Ruoff. *Nano Lett.* **9**, 4268 (2009).
43. N. Grossiord, J. Loos, O. Regev, C. E. Koning. *Chem. Mater.* **18**, 1089 (2006).
44. L. Vaisman, H. D. Wagner, G. Marom. *Adv. Colloid Interface Sci.* **128–130**, 37 (2006).
45. R. Bandyopadhyaya, E. Nativ-Roth, O. Regev, R. Yerushalmi-Rozen. *Nano Lett.* **2**, 25 (2001).
46. M. Zheng, A. Jagota, E. D. Semke, B. A. Diner, R. S. McLean, S. R. Lustig, R. E. Richardson, N. G. Tassi. *Nat. Mater.* **2**, 338 (2003).
47. M. D. Stoller, S. Park, Y. Zhu, J. An, R. S. Ruoff. *Nano Lett* **8**, 3498 (2008).
48. D. S. Yu, L. M. Dai. *J. Phys. Chem. Lett.* **1**, 467 (2010).
49. Y. K. Kim, D. H. Min. *Langmuir* **25**, 11302 (2009).
50. V. C. Tung, L. M. Chen, M. J. Allen, J. K. Wassei, K. Nelson, R. B. Kaner, Y. Yang. *Nano Lett.* **9**, 1949 (2009).

